1

2

3

Air calibration of an oxygen optode on an underwater glider

5

David P. Nicholson[1] and Melanie Feen[1,2]

7

1. Marine Chemistry and Geochemistry Department, Woods Hole Oceanographic Institution, Woods Hole, Massachusetts, USA

2. Geosciences Department, Skidmore College, Saratoga Springs, New York, USA

11

Corresponding email: dnicholson@whoi.edu

13

14

15

18

Running head: Glider oxygen air calibration

Abstract

An Aanderaa Data Instruments 4831 Oxygen optode was configured on an underwater glider such that the optode extended into the atmosphere during each glider surface interval enabling in situ calibration of the sensor by directly measuring the known partial pressure of the atmosphere. The approach, which has previously been implemented on profiling floats but not on gliders, was tested during a 15-day deployment at the New England shelf break in June 2016, a productive period during which surface O_2 saturation averaged 110%. Results were validated by shipboard Winkler O_2 calibration casts, which were used to determine a sensor gain factor of 1.055 ± 0.004. Consistent with profiling float observations, air measurements contain contamination from splashing water and/or residual seawater on the sensor face. Glider surface measurements were determined to be a linear combination of 36% of surface water and 64% atmospheric air. When correcting air measurements for this effect, a sensor gain correction of 1.055 ± 0.005 was calculated based on comparing glider air measurements to the expected atmospheric pO_2 calculated from atmospheric pressure and humidity data from a nearby NOAA buoy. Thus, the two approaches were in agreement and were both demonstrated to be accurate to within ±0.5%. We expect uncertainty in the air-calibration could be further reduced by increasing the vertical positioning of the optode, lengthening deployment time, or operating in waters with surface O_2 saturation closer to equilibrium.

Introduction

Oxygen is a central element in marine biogeochemistry as it is produced by photosynthesis and consumed by respiration. In the surface ocean, marine cycling of O_2 is coupled to the atmosphere via air-sea exchange processes. Measurements of dissolved oxygen are commonly used to infer rates of biogeochemical processes, including net community production (NCP),

43 which is the whole-ecosystem balance between photosynthesis and respiration (Emerson and

44 Bushinsky 2014). The net oxygen produced by NCP is stoichiometrically linked to excess

45 production of organic carbon that subsequently is available for export. O_2-based NCP estimates

46 thus are a critical means to quantify carbon export and the biological carbon pump.

47 Dissolved oxygen sensors are perhaps the most mature biogeochemical sensors used by the

48 oceanographic community. Over recent years, oxygen optodes have come to predominate in

49 oceanographic applications displacing polarographic Clark electrode type sensors. These sensors

50 are robust and reliable, yet, they are not perfect and are still subject to issues including drift after

51 factory calibration which can vary from undetectable rates to several percent per year.

52 Oxygen optodes operate on the underlying principle of quantifying the luminescence of a

53 metalloporphyrin (most commonly, platinum or rhuthenium) complex, the lifetime of which is a

54 function of quenching by molecular oxygen (Klimant et al. 1995; Tengberg et al. 2006; Quaranta

55 et al. 2012). Kinetics of quenching is described by the Stern-Volmer equation:

56

57 $$\frac{\tau}{\tau_0} = 1 + pO_2 K_{sv} \qquad (1)$$

58 where τ and τ_0 are the lifetime of the luminophore in the presence and absence of O_2, pO_2 is the

59 partial pressure of molecular oxygen and K_{sv} is the Stern-Volmer constant. A useful characteristic

60 of O_2 optodes is their ability to measure pO_2 in a range of media, including in seawater and in air.

61 One of the most promising techniques to address shortcomings in O_2 sensor accuracy is the

62 'air calibration' method that has recently been developed for application on Argo-style profiling

63 floats (Bittig and Körtzinger 2015; Johnson et al. 2015; Bushinsky et al. 2016). The approach

64 takes advantage of the fact that **O_2 optodes are capable of measuring O_2 partial pressure both**

65 **in fluid and in air. Periodic measurements of lower tropospheric air can serve as a reference**

3

66   **standard to track sensor accuracy and drift.** Dry atmosphere has a known and constant O_2

67   content, the air O_2 partial pressure ($pO_{2,a}$) can be precisely estimated knowing sea level pressure

68   (p_{atm}):

69

70    $$pO_{2,a} = (p_{atm} - p_{H_2O})\chi_{O_2} \quad \text{where} \quad p_{H_2O} = \phi p_{H_2O}^* \tag{2}$$

71

72   where χ_{O_2} is 0.20946, the dry air mixing ratio of O_2 (Glueckauf 1951), ϕ is relative humidity and

73    $p_{H_2O}^*$ is the saturated vapor pressure, a function of temperature and salinity (Wagner and Pruß

74   2002; Dickson et al. 2007).

75   By mounting optodes in a position such that the sensor is exposed to the air when a float is

76   at the surface, $pO_{2,a}$ can be measured during each surface interval. Any changes in apparent $pO_{2,a}$

77   over time can be attributed to sensor drift. The intercept of $\mathrm{d}(pO_{2,a})/dt$ with the deployment time

78   represents the initial sensor bias (Bushinsky et al. 2016). Here, we present the first application of

79   an air calibrating optode on a mobile platform, a Teledyne Webb Research G1 200m Slocum

80   Glider. The system was demonstrated during a 15-day deployment at the New England shelf

81   break.

82   **Materials and procedures**

83   *Air-calibration mounting*

84   An Aanderaa Data Instruments model 4831 oxygen optode (serial number 289, foil batch

85   1206EM) was re-configured on a Teledyne Webb Research 200m G1 Slocum glider such that the

86   optode was mounted fore of the glider tail (Fig 1A). When new, the optode was multipoint factory

87   calibrated by Aanderaa (calibration date 15 December, 2013) and all calculations were performed

88   using the modified Stern-Volmer equation (Uchida et al. 2008). When the glider is at the surface,

89   the modified mount holds the optode approximately 15 cm above the water line (Fig 1B). The

90   optode was positioned with the sensor foil was facing in the forward direction. This orientation

91   has a number of potential benefits. The vertical orientation reduces potential exposure to ambient

92   light compared to an upwards facing foil. Also, optode response time has been observed to depend

93   on sensor orientation relative to the direction of flow because when the sensor foil is facing directly

94   into the flow, diffusive boundary layer thickness is minimized and response time is optimized

95   (Bittig et al. 2014).
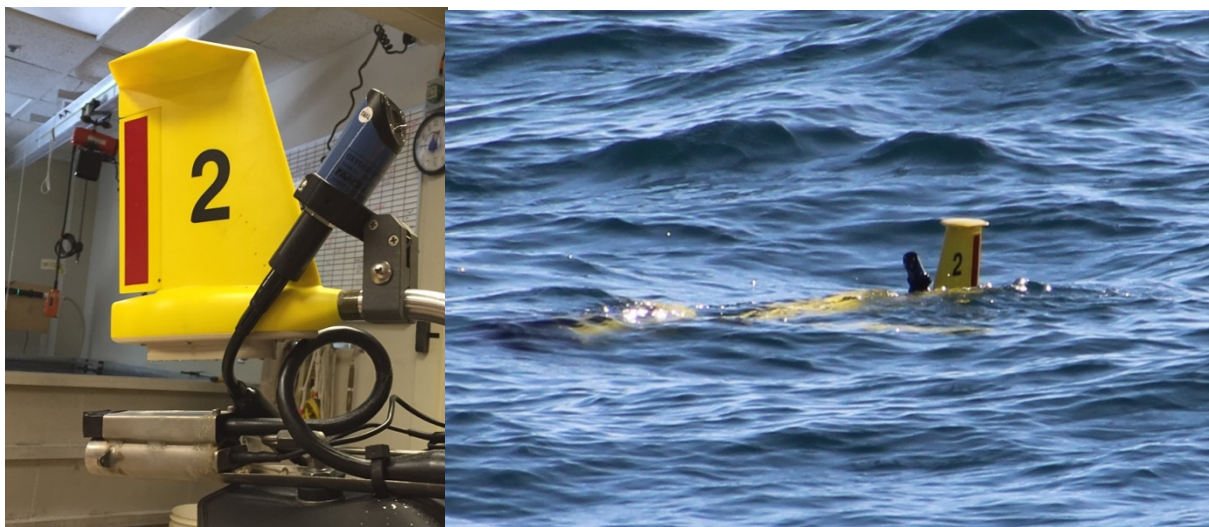
96

97   Figure 1: The prototype air-calibration mount is shown in the lab with glider rear fairing removed
98   (left) and at sea at the New England Shelf Break (right). The sensing foil is located on the angled
99   face of the sensor, facing into the direction of flow. This orientation both reduces interference
100   from incident light and improves sensor response time.
101

102   *Glider operations*

103   The Slocum glider was deployed on 02 June, 2016 from the R/V Tioga at 40.5°N 71°W

104   and was recovered on 18 June, 2016. In addition to the optode, the glider was equipped with a

105   Seabird CTD, WET Labs optical puck and Satlantic SUNA nitrate sensor. The glider conducted

106   three initial longer cross-shelf transects before rendezvousing with the R/V Endeavour which

107   arrived on site on 14 June, 2016. During the final four days, the glider conducted shorter sections

108   following a drifting Wire Walker as well as conducting calibration casts in coordination with the

109   ship on 15 and 17 June 2016 (Fig 2).

110
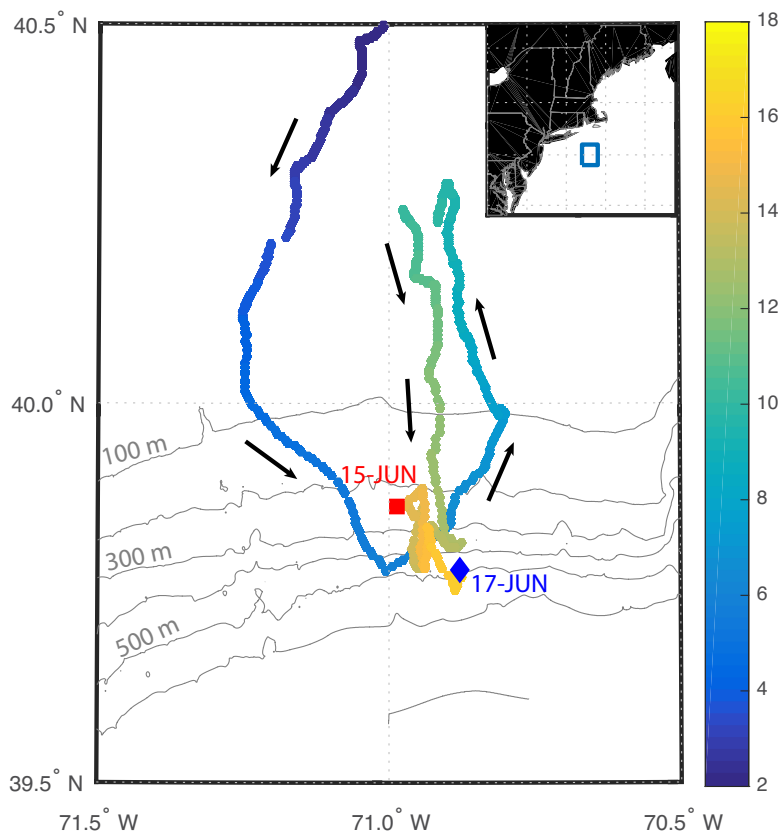
111

112   Figure 2: Map of glider deployment. The colorbar indicates day in June, 2016. Location of the
113   two calibration casts are shown in red and blue.
114
115   When water depth permitted, the glider repeatedly dove to its maximum rated depth of

116   200m. A paired 200 m dive and ascent lasted about 50 minutes. The glider does not breach the

117   surface on every ascent, instead inflecting downward just below the surface. The glider surfaces

118   about every third ascent. During surface intervals, the oxygen sensor was programmed to continue

119   to measure at a frequency of 1/4 Hz. The duration of each surface interval was about 10-15 minutes

120   during which O_2 measurement was interrupted for several minutes while the glider transmitted

121   data to shore. On average, 209 O_2 measurements were acquired during each surface interval.

122   *Mooring Data*

123   The expected $pO_{2,air}$ was calculated based on meteorological data collected from nearby

124   NOAA National Data Buoy Center Station 44008 located at 40.503°N 69.248°W and Eq. 2.

125   Hourly sea level pressure, air temperature and dewpoint data were used to calculate p_{atm}, ϕ and

126   p_{H_2O}. Measurement height for sensors on buoy 44008 were located at a height of 4 m. Values for

127   p_{H_2O} where corrected to a glider sensor height of 0.1 m using the method of Bittig et al. (2015).

128   The deployment spanned a range of low to moderate sea-states with windspeed varying from 0 –

129   12 m s^{-1} and significant wave height varying from 0.4 to 2.8 m.

130   *Winkler calibrations*

131   Prior to recovery, the glider rendezvoused with the R/V Endeavor. Two calibration casts

132   were conducted using the CTD on the R/V Endeavor on the mornings of 15 June 2016 and 17 June

133   2016. For each calibration cast, the glider was held at the surface in the vicinity of the Endeavor

134   (within ~500 m) and commanded to dive at the time when the CTD was lowered. Water was

135   collected in Niskin bottles at nominal depths of 200 m, 150 m, 100 m 50 m, the depth of chlorophyll

136   a maximum (44 m and 38 m, respectively), 30 m, 20 m, 5 m and 1 m. Dissolved Oxygen samples

137   for Winkler titration were collected in 125 m iodine titration flasks following standard operating

138   procedures (Langdon 2010). 1 m and 5 m samples were collected in triplicate while all other

139   depths were collected in duplicate.

140   Due to logistical limitations on the R/V Endeavor cruise, Winkler O_2 samples could not be

141   analyzed on the ship, but instead stored for the duration of the cruise in dark conditions with water

142   sealing flask necks until they were analyzed at WHOI on 21-22 June, 2016. While immediate

143   analysis is preferred, studies have demonstrated successful sample storage without biasing O_2

144   determinations for many days and even many months (Zhang et al. 2002; Langdon 2010),

145   Samples were titrated in the Nicholson Lab at WHOI using custom-designed Winkler titrator with

146   automated potentiometric endpoint detection. Standard deviation of replicates averaged ±0.28

147   μmol kg^{-1} or ±0.12%.

Assessment

Winkler O_2 evaluation

150   Cross-calibration against discrete Winkler O_2 observations has been, to-date, the preferred

151   method for calibration of glider oxygen sensors (Nicholson et al. 2008). The approach requires

152   close coordination of ship and autonomous operations to ensure a close match in time and space

153   between shipboard samples and the glider profile. Two calibration casts were conducted from the

154   R/V Endeavor, the first cast began at 11:52 UTC on 15 June 2016 was coordinated such that the

155   glider was located 200 m to the south of the ship's location. The second cast was at 11:05 UTC

156   on 17 June 2016. The glider was located 950 m to the east of the ship at the time of the cast. For

157   each calibration cast, the glider dive was initiated within five minutes of the start of the CTD cast.

158   Bottle samples were matched to their corresponding glider profiles by identifying the glider

159   data point nearest in density (σ_θ) space to avoid any noise introduced by vertical motions of internal

160   waves. Sensor lag time can introduce a historesis effect. Bottle values were matched to both the

161   descent and ascent profiles and the two values were averaged. A linear for paired values was

162   calculated both assuming (1) a linear fit; and (2) a linear fit with forced zero intercept (Table 1).

163   The latter method is equivalent to a gain correction. The raw glider O_2 measurements

164   ($[O_2]_w^{meas}$) were corrected ($[O_2]_w^{raw}$) using simple gain factor (G):

165 $$[O_2]_w^{meas} = G[O_2]_w^{raw} \tag{3}$$

166 Table 1: Winkler Calibration fit parameters. Best fit parameters are shown for each of two
167 calibration casts. Each fit is evaluated at 100% saturation. Sensor gain, used to correct the glider
168 optode is the inverse of the zero-intercept fit. Despite differences in best-fit slope and intercept,
169 each fit evaluated at atmospheric equilibrium resulted in a similar value.

	Linear fit		Zero intercept	Linear fit	Zero intercept	Gain
	m	b	M	$\Delta O_{2,w}^{raw}$ @100%	$\Delta O_{2,w}^{raw}$ @100%	G = 1/M
15 June	0.924	2.3 %	0.949	94.7 ±0.6%	94.9 ±0.6%	1.054 ±0.006
17 June	0.897	4.8 %	0.947	94.5 ±0.4%	94.7 ±0.4%	1.056 ±0.005
Combined	**0.913**	**3.3 %**	**0.948**	**94.6 ±0.3%**	**94.8 ±0.3%**	**1.055 ±0.004**

170 The gain factor, G, needed to correct glider O_2 observations is calculated as the inverse of the slope

171 of the fit line of Winkler O_2 versus raw glider O_2 with zero intercept (Figure 3). For both casts

172 combined, we calculate a gain of G_{all} = 1.055 ±0.004. The gain factor calculated independently

173 from the first and second cast were G_1 = 1.054 ±0.006 and G_2 = 1.056 ±0.005, respectively. R^2

174 was 0.994, 0.995 and 0.995 for combined data, calibration cast 1 and calibration cast 2,

175 respectively. When not forced to a zero intercept, the best linear fit had zero intercepts of 2.3 ±

176 2.5%, 4.8 ±1.6% and 3.3 ±1.4% for cast 1, cast 2 and combined data, respectively (Table 1). The

177 Post-recovery, a zero-point measurement of 1.14% was determined in the lab using 5 mg hydrogen

178 sulfite dissolved in 500 mL of DI water, as specified by the manufacturer. We suspect the

179 mismatch in zero intercept between the Winkler regression and lab measurement is because the

180 regression extrapolates, with no observations below 50% saturation and is heavily dependent on

181 the three data points at ~50% saturation.

182 The above regressions were calculated for O_2 percent saturation, but almost identical results were

183 calculated when concentration was used (data not shown). In summary, the calibration casts

184 showed a linear relationship between optode O_2 with the optode consistently measuring low,

185 correctable by multiplying by a gain factor of 1.055 ±0.004. Uncertainty ranges in each case are

186 based on standard error of the slope of the Type 1 Regression fit.
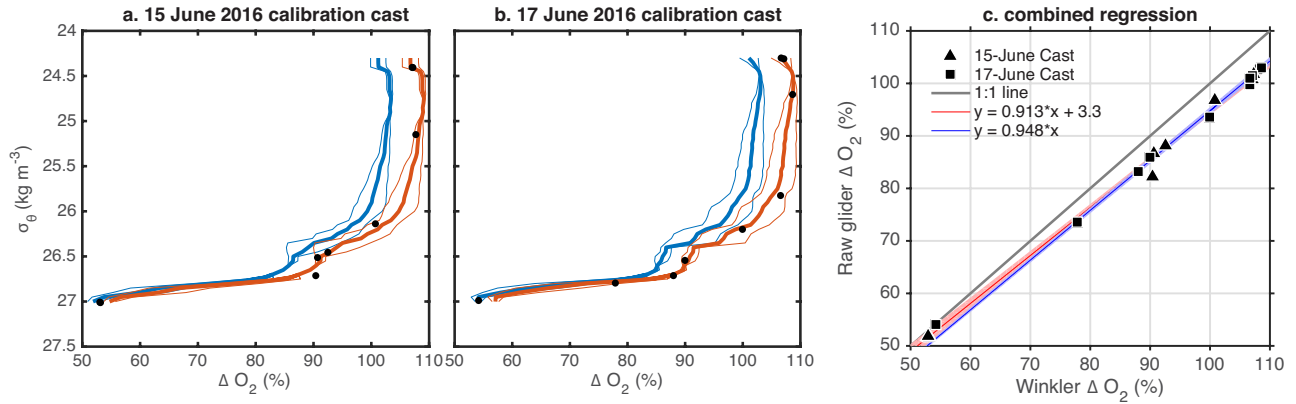
187

Figure 3: Glider O_2 from calibration casts on 15 June (a) and 17 June (b) prior to calibration (blue)
and post calibration (orange). Solid lines show average of dives and climbs (light traces). Black
symbols indicate Winkler bottle samples Panel c. shows best least squared linear fits with (blue)
and without (red) assuming a zero intercept. Two sigma uncertainty ranges are shown in blue and
red shading. Sensor gain (the inverse of the slope of the linear least square fit) was 1.055 ±0.004.

194   *O$_2$ air-calibration*

195   Winkler O$_2$ results provide a ground-truth for air calibration measurements. In the

196   following section we compare Winkler-calibrated glider O$_2$ observations to air O$_2$ measured by the

197   glider and inferred from buoy atmospheric measurements.

198   During each surface interval, the optode records measurements of the near-surface

199   atmosphere. We consider several factors that could contaminate this record such as (1) a response-

200   time adjustment period immediately after surfacing and (2) the influence of splashing water or

201   residual water on the sensor surface. Because the optode has a nominal response time around 30

202   seconds, it is likely that some time is needed after surfacing for measurements to stabilize. Air

203   measurements, binned by time since surfacing, indicate that this adjustment period lasted roughly

204   60 seconds before measurements stabilized (Fig 4). During this period, apparent air O$_2$ decreased

205   by about 4% on average.

206
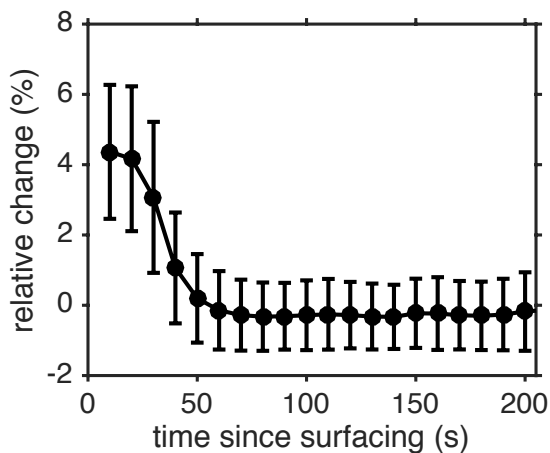
207

208   Figure 4: Change in measured air O$_2$ saturation (%) as a function of time since surfacing. The mean
209   air O$_2$ for each surface interval is subtracted. Error bars indicate the standard deviation for each
210   10 second time bin. Each bin contains, on average, 722 measurements.

211   Over the full deployment the glider recorded 35,177 total air O_2 measurements during 168

212 surface intervals. Compared to profiling floats, which surface infrequently and usually only make

213 a few measurements at the surface, the glider dataset provides a large amount information to

214 characterize O_2 optode sensor response at the surface. For each surface interval, we calculated the

215 measured value relative to standard air O_2 such that:

216

217          $\Delta O_{2,a}^{meas} = \dfrac{pO_{2,a}^{meas}}{pO_{2,ref}} - 1$ where $pO_2^{ref} = \chi_{O_2} p_{sat}$ (4)

218

219 where pO_2^{ref} is the partial pressure of O_2 at 1 atm and 100% saturated water vapor pressure (p_{sat}).

220 Note that $pO_{2,a}^{meas}/pO_2^{ref}$ is equal to $[O_2]_a^{meas}/[O_2]_{eq}$ where $[O_2]_{eq}$ is the equilibrium solubility

221 (Garcia and Gordon 1992). The expected O_2 anomaly for air ($\Delta O_{2,a}$) is defined analogously, using

222 NOAA buoy data and Eq. (2) such that deviations in $\Delta O_{2,a}$ from zero are due to changes in

223 atmospheric pressure and relative humidity.
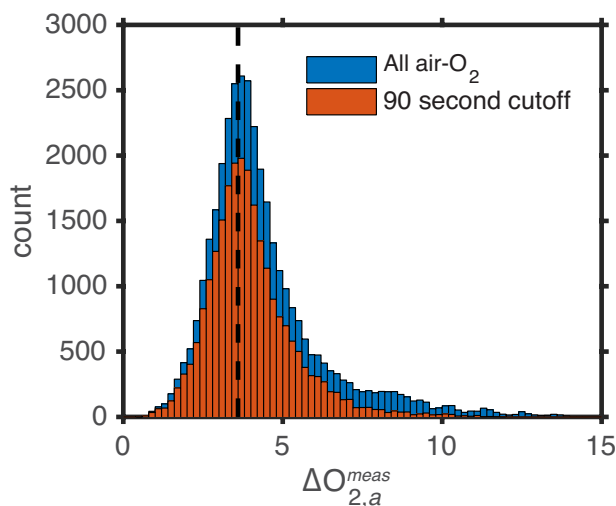
224

225 Figure 5: Histograms of $\Delta O_{2,a}^{meas}$ for all surface measurements ($n = 35,711$) and for surface
226 measurements excluding the first 90 seconds of each surface interval ($n = 24,199$). The vertical
227 dashed line indicates the mode value of $\Delta O_{2,a}^{meas} = 3.6\%$.

228   The distribution of air $\Delta O_{2,a}^{meas}$ measurements is skewed towards positive values (i.e.,

229   towards the observed positive surface water saturation) with a long tail on the upper end of the

230   distribution (Figure 5). Removing data from the first 90 seconds of each surface interval

231   significantly reduces the long tail, yet the distribution remains skewed. In both cases, the

232   distribution has the same mode (peak) bin at $\Delta O_{2,a}^{meas}$ = 3.6% which corresponds to the 28th and

233   32nd percentile for all measurements and for cutoff measurements, respectively. For comparison

234   to surface seawater measurements, we assign a single value for $\Delta O_{2,a}^{meas}$ for each surface interval

235   by taking the 32nd percentile of measurements from a surface interval after excluding the first 90

236   seconds of observations. Corresponding surface seawater O_2 was calculated by taking the average

237   of observations from 1 - 2.5 m depth during the ascent immediately prior to the surface interval.

238   A descent value was calculated by linearly interpolating in time the surface (1 - 2.5m) averages

239   from non-surfacing periods to the average time of each surface interval. Descents immediately

240   after surface intervals were not used because a time-lag effect, reverse of that observed

241   immediately after surfacing, was observed during these dives, biasing surface values low over the

242   upper several meters. Similar to what has been observed on profiling floats (Bittig and Körtzinger

243   2015; Johnson et al. 2015), we found a correlation between $\Delta O_{2,a}^{meas}$ and the surface water O_2

244   saturation, $\Delta O_{2,w}^{meas}$ with a slope of 0.36 ±0.03 and R^2 of 0.44 (Fig 6). The slope of 0.36 is

245   comparable, but somewhat higher than published values for profiling floats of 0.22 (Bittig and

246   Körtzinger 2015) and 0.29 (Johnson et al. 2015). Following Bittig and Körtzinger (2015) we

247   corrected measured O_2 such that:

248

249        $$\Delta O_{2,a}^{corr} = \frac{\Delta O_{2,a}^{meas} - m\left(\Delta O_{2,w}^{meas}\right)}{1-m}$$ (5)

250

                                                                                                                                13

251   where $\Delta O_{2,a}^{corr}$ is the corrected air measurement and m is the slope of 0.36. After completing the

252   above correction, the difference between glider measured air and the expected O_2 of air based on

253   buoy atmospheric pressure measurements $(\Delta O_{2,a}^{corr} - \Delta O_{2,a}^{buoy})$ was with error of zero $(\Delta O_{2,a}^{corr} -$

254    $\Delta O_{2,a}^{buoy} = -0.01 \pm 1.18\%)$, where the uncertainty range is based on one standard deviation (Fig 7).

255   Put in other terms, when $\Delta O_{2,a}^{corr}$ is calculated from raw $\Delta O_{2,a}^{raw}$ instead of $\Delta O_{2,a}^{corr}$, the gain

256   calculated from air O_2 is $(\Delta O_{2,a}^{buoy} - 1)/(\Delta O_{2,a}^{raw} - 1)$ and equal to 1.055, within rounding error

257   of the G calculated from Winkler calibration.

258   If each surface interval is considered an independent estimate of $\Delta O_{2,a}^{corr}$, then the

259   calculated standard error of the mean is 0.09%. $\Delta O_{2,a}^{corr}$ was weakly, but significantly correlated

260   with $\Delta O_{2,a}^{buoy}$ ($R^2 = 0.035$, $p = 0.02$) indicating that the glider air calibration may be able to track

261   small variations in atmospheric pressure. The low correlation is not unexpected, as $\Delta O_{2,a}^{buoy}$ has a

262   very small dynamic range ($-0.6 \pm 0.6\%$).
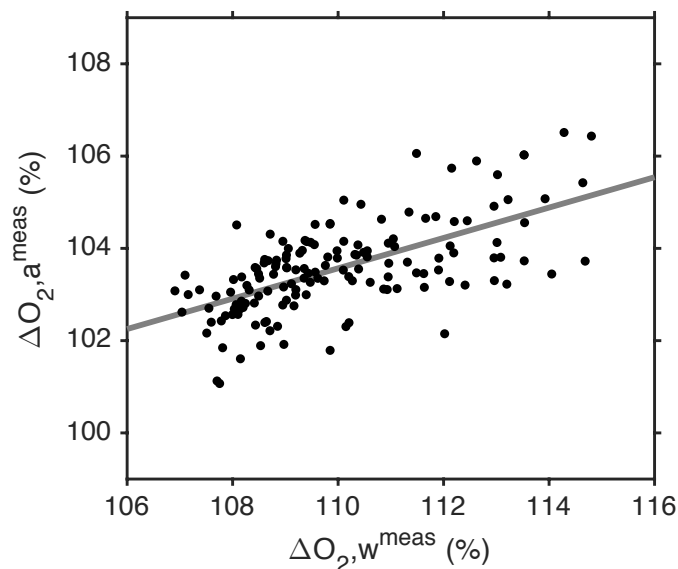
263
264 Figure 6: Surface oxygen saturation anomaly versus measured air anomaly showed a linear
265 relationship with a slope of 0.36 and R^2 of 0.44.
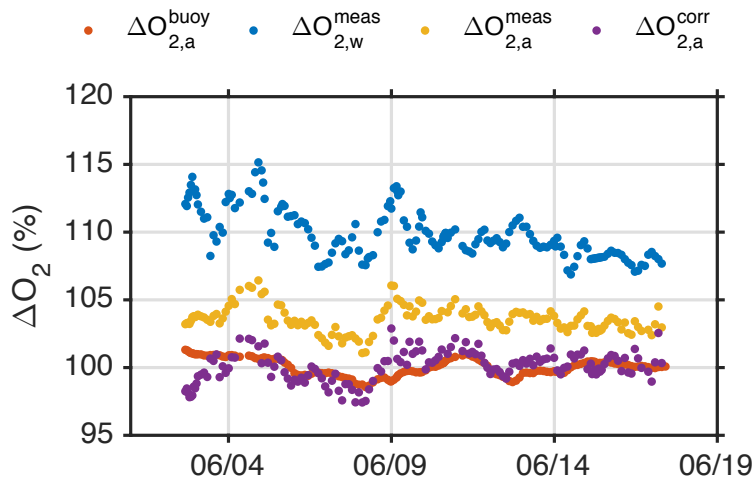
266

Figure 7: Initial glider air O_2 measurements ($\Delta O_{2,a}^{meas}$; yellow) were corrected ($\Delta O_{2,a}^{corr}$; purple) for influence from surface water O_2 saturation ($\Delta O_{2,w}^{meas}$; blue). Corrected ($\Delta O_{2,a}^{corr}$) values, when using a gain of 1.055, were within error of the expected atmospheric O_2 content as determined from buoy sea level pressure measurements ($\Delta O_{2,a}^{buoy}$; orange).

Discussion

In this study, we demonstrated that a newly developed air calibration method for dissolved oxygen optodes produced results in good agreement with ship-based calibration casts with Winkler bottle O_2 titrations. Each method determined that a gain factor of 1.055 was necessary to correctly calibrate the glider optode. Accurate air-calibration assessment must take into account the influence of surface ocean saturation, likely due to splashing waves and spray, that cause the optode to measure a combination of atmosphere and surface ocean during surface intervals. Following Bittig et al. (2015) we determined a relative contribution of 64% air ($\Delta O_{2,a}^{meas}$) and 36% for surface water ($\Delta O_{2,w}^{meas}$). Given the high biologically driven supersaturation of 7-15% observed during the glider deployment, the above correction resulted in the corrected air O_2 measurement being about a 4% lower than raw measurements.

15

282   *Air calibration uncertainty analysis*

283   Uncertainty in the absolute accuracy of the air calibration method stems from several

284   potential sources, including the scatter in $\Delta O_{2,a}^{corr}$, uncertainty in the sea level pressure and humidity

285   data used to calculate $\Delta O_{2,a}^{buoy}$ and uncertainty in magnitude of surface water influence. Here, we

286   assess the contribution of these sources of uncertainty to overall uncertainty in the air calibration

287   method. In the section above, we determined a standard error of the mean of $\pm 0.09\%$ for $\Delta O_{2,corr}$,

288   but additional potential sources of bias increase the true uncertainty. The accuracy in quantifying

289    $\Delta O_{2,a}^{buoy}$ is calculated from propagating a ± 1 hPa typical uncertainty for p_{atm} and a $\pm 5\%$ uncertainty

290   for p_{H_2O} in Eq. (2) resulting in an uncertainty of $\pm 0.11\%$ in $\Delta O_{2,a}^{buoy}$. The greatest source of

291   uncertainty stems from uncertainty in m (Eq. 5). Propagating the ± 0.03 uncertainty in m through

292   Eq. (5) results in a $\pm 0.5\%$ uncertainty in $\Delta O_{2,a}^{corr}$. Thus, we consider $\pm 0.5\%$ to the best measure of

293   overall uncertainty for the accuracy of the air O_2 glider calibration. Applied to the gain factor, the

294   uncertainty equates to 1.055 ± 0.005, similar in magnitude to the ± 0.004 uncertainty determined

295   from Winkler calibration.

296   In practice, the magnitude of this uncertainty will depend both on the magnitude of m (i.e.,

297   lower m will reduce uncertainty) as well as on saturation anomaly of the surface ocean ($\Delta O_{2,w}^{meas}$)

298   such that error will be smaller when surface water is closer to equilibrium (Fig 8). For conditions

299   in most of the open ocean where $\Delta O_{2,w} - \Delta O_{2,a}$ is less than 5%, this source of error is significantly

300   reduced. Further reduction in uncertainty could be achieved by reducing m by increasing the

301   mounting height of the air-calibration optode.

302   The accuracy we achieved with the glider deployment are comparable to recent results

303   from profiling floats. Bittig et al. (2015) reported accuracy of $\pm 1\%$, Johnson et al. (2015) reported

304   <1% error. When comparing air calibration to Winkler calibration across eight floats Bushinsky

305   et al. (2016) reported an −0.5 ± 0.7% range. These float studies also investigated long term drift

306   in optodes which was determined to generally be less than 0.5% y^{-1}. Over the course of a 15-day

307   deployment, this amounts to an undetectable change of 0.02%, so we are unable to evaluate sensor

308   drift in this study. For longer glider deployments, such as year-long deployments at Ocean

309   Observing Initiative (OOI) sites, quantifying drift likely is achievable.

310

311
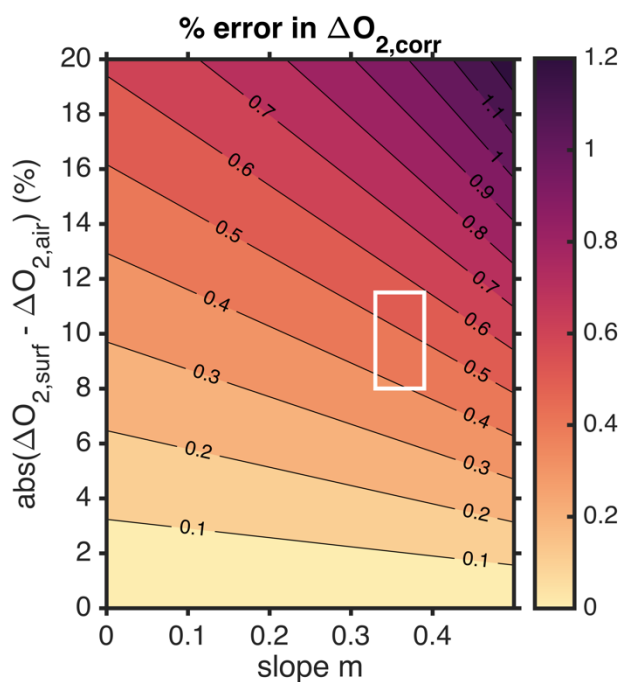
312

Figure 8: Error associated with a 0.03 uncertainty in (m) the surface water contribution to
$\Delta O_{2,a}^{corr}$ (see Eq. 5) as a function of the difference between air and surface water saturation. The
white box indicates the range of observations from this study.

Comments and recommendations

318   The application of air calibration on underwater gliders opens up a range of exciting

319   applications. Foremost, improved control on sensor accuracy will improve oxygen-based net

320   community production estimates from gliders, which rely and precise characterization of air-sea

17

321   O_2 fluxes and thus are particularly sensitive to any biases in quantifying surface O_2 saturation

322   (Emerson and Bushinsky 2014). Additionally, adding O_2 air calibration to a glider enables the

323   possibility of autonomous cross-calibration of observing networks. For example, within an OOI

324   Array, a glider equipped with an air calibrating optode could be piloted to dive at the location of

325   moorings and other mobile assets that are equipped with oxygen sensors to create a cross-

326   calibrated observing network.

327   We conclude that O_2 air calibration on gliders is a robust new tool for in situ calibration

328   of dissolved oxygen sensors to 0.5% or better accuracy. Achieving this level of accuracy

329   requires attention to two primary potential sources of bias including (1) A transient sensor

330   response when the optode crosses the sea surface interface, which was observed to stabilize after

331   about 50 seconds, and (2) the observed influenced of surface water saturation on air

332   measurements, likely due to splashing waves. Air measurements must be corrected for this

333   influence when surface saturation departs significantly from air pO_2 (i.e., using Eq. 5). We

334   recommend that the correction factor, *m*, should preferably be determined directly for each given

335   glider deployment, and literature values from this, or other sources should not be assumed

336   applicable. An increased optode mount height, coupled with operating in open ocean conditions

337   where surface O_2 saturation is typically within ±5% of equilibrium likely would reduce

338   uncertainty in sensor accuracy to below 0.25%.

339   The air calibration method appears to be approaching the accuracy and precision

340   achievable by traditional Winkler calibrations. For studies where surface oxygen saturation is of

341   primary importance, air calibration can provide similar accuracy while avoiding the logistical

342   constraints of conducting Winkler titrations and calibration casts. However, we feel there still is

343   an important role for Winkler titrations for several reasons, including (1) Air calibration is still a

344   new approach and it should continue to be validated over a wider range of oceanographic

345   conditions; and (2) Air calibration only provides a calibration point for surface O_2 saturation.

346   Uncertainty about the accuracy and drift of optodes at lower oxygen concentrations remain,

347   requiring further investigation.

348

349

350

351

352 **References**

353 Bittig, H. C., B. Fiedler, R. Scholz, G. Krahmann, and A. Körtzinger. 2014. Time response of

354   oxygen optodes on profiling platforms and its dependence on flow speed and temperature.

355   Limnol. Oceanogr. Methods **12**: 617–636. doi:10.4319/lom.2014.12.617

356 Bittig, H. C., and A. Körtzinger. 2015. Tackling Oxygen Optode Drift: Near-Surface and In-Air

357   Oxygen Optode Measurements on a Float Provide an Accurate in Situ Reference. J.

358   Atmospheric Ocean. Technol. **32**: 1536–1543. doi:10.1175/JTECH-D-14-00162.1

359 Bushinsky, S. M., S. R. Emerson, S. C. Riser, and D. D. Swift. 2016. Accurate oxygen

360   measurements on modified Argo floats using in situ air calibrations. Limnol. Oceanogr.

361   Methods. doi:10.1002/lom3.10107

362 Dickson, A. G., C. L. Sabine, and J. R. Christian. 2007. Guide to Best Practices for Ocean CO2

363   Measurements. Report North Pacific Marine Science Organization.

364 Emerson, S. R., and S. Bushinsky. 2014. Oxygen concentrations and biological fluxes in the open

365   ocean. Oceanography **27**: 168–171. doi:10.5670/oceanog.2014.20

366 Garcia, H. E., and L. I. Gordon. 1992. Oxygen solubility in seawater: Better fitting equations.

367   Limnol. Oceanogr. **37**: 1307–1312. doi:10.4319/lo.1992.37.6.1307

368 Glueckauf, E. 1951. The composition of atmospheric air, p. 1–11. *In* Compendium of

369   Meteorology. American Meteorology Society.

370 Johnson, K. S., J. N. Plant, S. C. Riser, and D. Gilbert. 2015. Air Oxygen Calibration of Oxygen

371   Optodes on a Profiling Float Array. J. Atmospheric Ocean. Technol. **32**: 2160–2172.

372   doi:10.1175/JTECH-D-15-0101.1

373 Klimant, I., V. Meyer, and M. Kühl. 1995. Fiber-optic oxygen microsensors, a new tool in aquatic

374   biology. Limnol. Oceanogr. **40**: 1159–1165. doi:10.4319/lo.1995.40.6.1159

375   Langdon, C. 2010. Determination of dissolved oxygen in seawater by Winkler titration using the

376   amperometric technique. 14. 14 IOCCP.

377   Nicholson, D., S. Emerson, and C. C. Eriksen. 2008. Net community production in the deep

378   euphotic zone of the subtropical North Pacific gyre from glider surveys. Limnol. Oceanogr.

379   **53**: 2226–2236. doi:10.4319/lo.2008.53.5_part_2.2226

380   Quaranta, M., S. M. Borisov, and I. Klimant. 2012. Indicators for optical oxygen sensors. Bioanal.

381   Rev. **4**: 115–157. doi:10.1007/s12566-012-0032-y

382   Tengberg, A., J. Hovdenes, H. J. Andersson, and others. 2006. Evaluation of a lifetime-based

383   optode to measure oxygen in aquatic systems. Limnol. Oceanogr. Methods **4**.

384   Uchida, H., T. Kawano, I. Kaneko, and M. Fukasawa. 2008. In situ calibration of optode-based

385   oxygen sensors. J. Atmospheric Ocean. Technol. **25**: 2271–2281.

386   doi:10.1175/2008JTECHO549.1

387   Wagner, W., and A. Pruß. 2002. The IAPWS Formulation 1995 for the Thermodynamic Properties

388   of Ordinary Water Substance for General and Scientific Use. J. Phys. Chem. Ref. Data **31**:

389   387–535. doi:10.1063/1.1461829

390   Zhang, J.-Z., G. Berberian, and R. Wanninkhof. 2002. Long-term storage of natural water samples

391   for dissolved oxygen determination. Water Res. **36**: 4165–4168. doi:10.1016/S0043-

392   1354(02)00093-3

393

394

Table and Figure Captions

Table 1: Winkler Calibration fit parameters. Best fit parameters are shown for each of two calibration casts. Each fit is evaluated at 100% saturation. Sensor gain, used to correct the glider optode is the inverse of the zero-intercept fit. Despite differences in best-fit slope and intercept, each fit evaluated at atmospheric equilibrium resulted in a similar value.

Figure 1: The prototype air-calibration mount is shown in the lab with glider rear fairing removed (left) and at sea at the New England Shelf Break (right). The sensing foil is located on the angled face of the sensor, facing into the direction of flow. This orientation both reduces interference from incident light and improves sensor response time.

Figure 2: Map of glider deployment. The colorbar indicates day in June, 2016. Location of the two calibration casts are shown in red and blue.

Figure 3: Glider O_2 from calibration casts on 15 June (a) and 17 June (b) prior to calibration (blue) and post calibration (orange). Solid lines show average of dives and climbs (light traces). Black symbols indicate Winkler bottle samples Panel c. shows best least squared linear fits with (blue) and without (red) assuming a zero intercept. Two sigma uncertainty ranges are shown in blue and red shading. Sensor gain (the inverse of the slope of the linear least square fit) was 1.055 ±0.004.

Figure 4: Change in measured air O_2 saturation (%) as a function of time since surfacing. The mean air O_2 for each surface interval is subtracted. Error bars indicate the standard deviation for each 10 second time bin. Each bin contains, on average, 722 measurements.

Figure 5: Histograms of $\Delta O_{2,a}^{meas}$ for all surface measurements (n = 35,711) and for surface measurements excluding the first 90 seconds of each surface interval (n = 24,199). The vertical dashed line indicates the mode value of $\Delta O_{2,a}^{meas}$= 3.6%.

Figure 6: Surface oxygen saturation anomaly versus measured air anomaly showed a linear relationship with a slope of 0.36 and R^2 of 0.44.

Figure 7: Initial glider air O_2 measurements ($\Delta O_{2,a}^{meas}$; yellow) were corrected ($\Delta O_{2,a}^{corr}$; purple) for influence from surface water O_2 saturation ($\Delta O_{2,w}^{meas}$; blue). Corrected ($\Delta O_{2,a}^{corr}$) values, when using a gain of 1.055, were within error of the expected atmospheric O_2 content as determined from buoy sea level pressure measurements ($\Delta O_{2,a}^{buoy}$; orange).

Figure 8: Error associated with a 0.03 uncertainty in (m) the surface water contribution to $\Delta O_{2,a}^{corr}$ (see Eq. 5) as a function of the difference between air and surface water saturation. The white box indicates the range of observations from this study.